2-24-2022

Influence of Hydrophobicity on Excitonic Coupling in DNA-Templated Indolenine Squaraine Dye Aggregates

Olga A. Mass
Boise State University

Christopher K. Wilson
Boise State University

German Barcenas
Boise State University

Lan Li
Boise State University

Bernard Yurke
Boise State University

See next page for additional authors

Publication Information

Mass, Olga A.; Wilson, Christopher K.; Barcenas, German; Terpetschnig, Ewald A.; Obukhova, Olena M.; Kolosova, Olga S.; . . . and Lee, Jeunghoon. (2022). "Influence of Hydrophobicity on Excitonic Coupling in DNA-Templated Indolenine Squaraine Dye Aggregates". *The Journal of Physical Chemistry C, 126*(7), 3475-3488. https://doi.org/10.1021/acs.jpcc.1c08981

THE JOURNAL OF PHYSICAL CHEMISTRY C
A JOURNAL OF THE AMERICAN CHEMICAL SOCIETY

pubs.acs.org/JPCC

Article

Influence of Hydrophobicity on Excitonic Coupling in DNA-Templated Indolenine Squaraine Dye Aggregates

Olga A. Mass, Christopher K. Wilson, German Barcenas, Ewald. A. Terpetschnig, Olena M. Obukhova, Olga S. Kolosova, Anatoliy L. Tatarets, Lan Li, Bernard Yurke, William B. Knowlton, Ryan. D. Pensack,* and Jeunghoon Lee*

Cite This: *J. Phys. Chem. C* 2022, 126, 3475−3488

Read Online

ACCESS | Metrics & More | Article Recommendations | Supporting Information

ABSTRACT: Control over the strength of excitonic coupling in molecular dye aggregates is a substantial factor for the development of technologies such as light harvesting, optoelectronics, and quantum computing. According to the molecular exciton model, the strength of excitonic coupling is inversely proportional to the distance between dyes. Covalent DNA templating was proved to be a versatile tool to control dye spacing on a subnanometer scale. To further expand our ability to control photophysical properties of excitons, here, we investigated the influence of dye hydrophobicity on the strength of excitonic coupling in squaraine aggregates covalently templated by DNA Holliday Junction (DNA HJ). Indolenine squaraines were chosen for their excellent spectral properties, stability, and diversity of chemical modifications. Six squaraines of varying hydrophobicity from highly hydrophobic to highly hydrophilic were assembled in two dimer configurations and a tetramer. In general, the examined squaraines demonstrated a propensity toward face-to-face aggregation behavior observed via steady-state absorption, fluorescence, and circular dichroism spectroscopies. Modeling based on the Kühn−Renger−May approach quantified the strength of excitonic coupling in the squaraine aggregates. The strength of excitonic coupling strongly correlated with squaraine hydrophobic region. Dimer aggregates of dichloroindolenine squaraine were found to exhibit the strongest coupling strength of 132 meV (1065 cm^{-1}). In addition, we identified the sites for dye attachment in the DNA HJ that promote the closest spacing between the dyes in their dimers. The extracted aggregate geometries, and the role of electrostatic and steric effects in squaraine aggregation are also discussed. Taken together, these findings provide a deeper insight into how dye structures influence excitonic coupling in dye aggregates covalently templated via DNA, and guidance in design rules for exciton-based materials and devices.

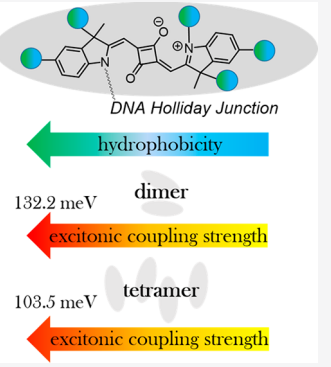

INTRODUCTION

When neighboring dye molecules (chromophores) are excited, their local excited states can couple with a molecular exciton (also known as a Frenkel exciton) with excitation energy shared between the dyes in a wave-like manner. Observation of excitonic coupling and delocalization enabling efficient energy transfer in natural photosynthetic dye aggregates motivated the development of exciton-based applications and devices that encompass artificial photosynthesis,[1−3] organic optoelectronics,[4,5] and nanoscale computing.[6−10] The functionality of these applications is governed by the ability to control and enhance the strength of excitonic coupling. According to the Kasha molecular exciton model,[11,12] the excitonic hopping parameter $J_{m,n}$[13−15] characterizes the strength of the Coulombic interaction responsible for the electronic transitions' interaction and thereof can quantitatively describe the strength of excitonic coupling. To facilitate the discussion, we treat the Coulombic interaction approximately as a dipole−dipole interaction following the approach of McRae and Kasha.[12] In this case, the magnitude of $J_{m,n}$ is inversely proportional to the cube of the distance between transition dipole moments constituted in the dyes of an aggregate (eq 1). As such, an organized and dense dye packing is an essential prerequisite for strong excitonic coupling that enables exciton delocalization. The magnitude of $J_{m,n}$ is given by

$$J_{m,n} = \frac{1}{4\pi\varepsilon\varepsilon_0}\left(\frac{\mu_m\cdot\mu_n}{|R_{m,n}|^3} - \frac{(\mu_m\cdot R_{m,n})(\mu_n\cdot R_{m,n})}{|R_{m,n}|^5}\right) \quad (1)$$

where μ_m and μ_n are the transition dipoles for the dyes at sites m and n, $R_{m,n}$ is the vector connecting dyes at sites m and n, ε_0 is the permittivity of the vacuum, and ε is the relative dielectric constant of the medium.

With the dye concentration approaching the solubility limit in a solvent, dyes can be brought in proximity and form a non-

Received: October 14, 2021
Revised: January 15, 2022
Published: February 10, 2022

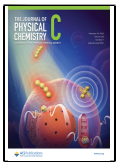

covalent complex maintained by weak van der Waals forces, that is, a molecular aggregate. Aggregation of free dyes in solution occurs spontaneously and can result in dimers, a mixture of monomers and dimers, and higher-order aggregates.[16,17] To gain more precise control over the number and position of dyes, various templates have been employed to assemble dye aggregates. Among different types of templates, DNA has been proven to be a powerful tool in organizing dyes into aggregates. The versatility of DNA as a template in the field of DNA nanotechnology stems from the relatively straightforward DNA self-assembly that relies on the complementary nature of four Watson−Crick base pairs allowing one to predict the shape of the template and location of dyes.[18−21] DNA can template dyes into dye−dye aggregates whether they are covalently or non-covalently attached to the DNA. A non-covalent method when dyes non-covalently bind to DNA is indeed simpler in implementation. While non-covalent binding to DNA was employed to create extended arrays of dyes,[22−27] the number of dyes in the aggregate and their exact position remained elusive.

The covalent DNA templating is based on attaching dyes via linkers to nucleobases or the backbone of single-stranded DNA, followed by self-assembly of complementary strands into double-stranded DNA. As a result, the number of dyes per DNA construct is strictly defined, with the predictable location of the dyes relative to the DNA backbone.[28−47] The advantage of covalent DNA templating over dye spacing was demonstrated by Nicoli et al. who examined how base pair (bp) separation corresponding to ∼3.5 Å increments affects dimerization ability of Cy3 dyes covalently attached to DNA.[28] Furthermore, Cunningham et al. studied excitonic coupling as a function of bp separation and estimated the excitonic coupling strength in a Cy3 dimer to be 33.0 meV (266 cm^{-1}) and 18.6 meV (150 cm^{-1}) for 0 and 1 bp separation, respectively.[32] A diversity of dye aggregates covalently templated to DNA can be further extended by utilizing more complex DNA architectures such as a branched 3-way junction, a 4-way junction, DNA nanobreadboards, and DNA origami.[20] The examples of high-order DNA templates include Probst's work on the aggregates of alkynylpyrene and perylenediimide covalently templated to the branch point of a three-way DNA junction, and Mazuski's work on Cy5 dimers attached to a DNA wire of two cross-linked DNA duplexes.[48,49] An additional special feature of DNA covalent templating that offers distinct advantage over both spontaneous aggregation and aggregation via non-covalent DNA templating has been recently demonstrated by Barclay et al. with a dimer aggregate of water-soluble squaraine rotaxane created via covalent tethering to a DNA Holliday Junction (DNA HJ).[50] This work uncovered the ability of DNA covalent templating to bring dyes of varying aqueous solubilities in proximity and promote their aggregation. Consequently, aggregation of a broader scope of dye chemical structures can be explored via covalent DNA templating.

In the past few years, our group has created dye aggregates via covalent templating to linear DNA and 4-arm DNA, that is, DNA HJ.[7,51−53] In the DNA HJ, dyes are covalently attached to the four strand branch point allowing dye aggregation in a dimer, trimer, or a tetramer form. Initially starting with the aggregates of Cy5, we recently extended toward aggregates of commercial indolenine squaraine dyes.[50,54] Squaraines structurally resemble the Cy5 dye, but feature a squarate moiety incorporated into the center of a pentamethine bridge between heterocyclic rings. Like Cy5, squaraines exhibit excellent spectral characteristics evident in their strong absorption in the visible region with a molar extinction coefficient in the range of 200,000−250,000 cm^{-1} M^{-1} and strong emission. We demonstrated that both Cy5 and squaraine dyes are capable of strong excitonic coupling and delocalization in their dimer and tetramer aggregates. However, squaraines offer advantages over Cy5 that include increased rigidity and photostability. In addition, squaraines can be synthesized with a diverse number and structure of substituents. While a dye's photophysical properties stem mainly from the chromophore core structure, varying the structure of side substituents can be used to fine-tune dye packing and, hence, enhance excitonic coupling.

While aggregation of many dye families was investigated in aqueous solution,[23,55−62] the studies mainly focused on the dye propensity to aggregate rather than their ability toward strong excitonic coupling. To our knowledge, only one report by the group of Armitage attempted to evaluate the influence of a dye peripheral structure on the excitonic coupling in cyanine aggregates templated via non-covalent binding to DNA. This study demonstrated that, in general, hydrophobic dyes have a tendency to exhibit strong excitonic coupling. However, a direct correlation between dye hydrophobicity, intermolecular distances, and the resulting strength of excitonic coupling in dye aggregates has not been provided. This study was also conducted with four cyanine dyes of similar hydrophobicity constraining the ability to fully reveal the influence of dye structures on the photophysical properties of their aggregates. This limitation presumably originates from the narrow range of dyes suitable for non-covalent DNA templating (as well as for spontaneous aggregation) excluding both insoluble and highly water-soluble dyes. The former tends to form higher-order aggregates complicating the analysis of precipitates from solution, while the latter, if they aggregate at all, have a large monomer population and require high dye concentrations that impede spectral measurements at high optical density. Also, a narrow set of explored structural variations for the same set of dyes is often due to the limitations of synthetic structural modifications.

In this paper, taking advantage of covalent DNA templating, we examine the influence of dye hydrophobicity on the aggregation behaviors and excitonic coupling strength within a wide range of indolenine-based squaraine dyes. Owing to the diversity of synthetically accessible indolenine squaraine structures, we chose six squaraines that differ by variations in the polarity and number of their substituents, including methyl, chloro, sulfo, and sulfobutyl groups. The squaraines were further categorized as overall hydrophobic or hydrophilic based on their relative water solubility. The dyes were covalently tethered to single-stranded DNA used to form a DNA HJ. The DNA HJ was used to template the dyes in the form of dimer (both transverse and adjacent) and tetramer aggregates. Both strength of excitonic coupling and aggregate geometry were quantified via Kühn−Renger−May modeling of the dye aggregate optical properties. We correlated hydrophobicity in terms of a partitioning coefficient derived via density functional theory (DFT) calculations with a center-to-center distance and strength of excitonic coupling. Structural modification of squaraine side substituents allowed us to vary the center-to-center distance between the dyes on the Angstrom level. Our findings indicate that dye hydrophobicity appears to play a predominant role in the intermolecular distance and strength of excitonic interactions in DNA-templated squaraine dye

https://doi.org/10.1021/acs.jpcc.1c08981
J. Phys. Chem. C 2022, 126, 3475−3488

aggregates. The aggregates with the strongest excitonic coupling observed in this work originate from a dichloro derivative, which is the most hydrophobic and with minimal dye sterics that would frustrate aggregation. We believe that our findings will facilitate a deeper understanding of how dye structures influence aggregate optical properties, particularly covalently templated via DNA, and may serve as a stepping stone toward design rules for exciton-based materials and devices.

METHODS

Dye Synthesis. Custom indolenine squaraine dyes were obtained from SETA BioMedicals, (Urbana-Champaign, IL). The synthesis of indolenine squaraines NHS-esters **SQ-Sl$_3$** and **SQ-Sl$_5$** was reported previously.[62] The synthetic procedures for new indolenine squaraines NHS-esters **SQ-H$_2$**, **SQ-Cl$_2$**, **SQ-Me$_2$**, and **SQ-Sl$_2$** are reported in Section S1.

Synthesis of DNA Constructs. DNA oligomers internally functionalized with a custom squaraine (SETA BioMedicals, Urbana-Champaign, IL) via a nucleosidic C6 dT sequence modifier and purified via dual high-performance liquid chromatography were purchased from Integrated DNA Technology, Inc (Coralville, IA). Non-functionalized DNA oligomers purified by standard desalting were purchased from Integrated DNA Technology, Inc. All DNA oligomers were rehydrated in ultrapure water (Barnstead Nanopure, Thermo Scientific) to prepare 100 μM stock solutions. Concentrations of the DNA samples were determined spectroscopically on a NanoDrop One Microvolume UV−Vis spectrometer (Thermo Scientific) using calculated extinction coefficients. DNA HJs were prepared by combining equimolar amounts of complimentary oligomers in 1× TBE, 15 mM $MgCl_2$ buffer solution to a final DNA concentration 1.5 μM. All DNA samples were annealed using a Mastercycler Nexus PCR cycler (Eppendorf) according to the following protocol: 4 min at 95 °C, followed by cooling ramps: 0.1 °C per 15 s from 94 to 64 °C, and 10 °C per 1 min from 64 °C to room temperature. For the fluorescence measurements, the DNA samples were further diluted to a 0.5 μM DNA concentration.

Optical Characterization. The UV−Vis spectra were recorded in duplicates at room temperature on a dual-beam Cary 5000 UV−Vis−NIR spectrophotometer (Agilent Technologies) in a quartz cuvette with a 1 cm path length (Starna). The absorbtion spectra were monitored over a 230−800 nm wavelength range. Circular dichroism (CD) measurements were performed on a JASCO-J810 spectropolarimeter. DNA samples (120 μL) were transferred into a 1 cm path length quartz cuvette (Jasco). The spectra were recorded over a 230−800 nm wavelength range (three scans per sample were averaged) at a speed of 200 nm min^{-1}. The steady-state fluorescence spectra were obtained using a Horiba PTI QuantaMaster 400 spectrofluorometer (Horiba Scientific) in a 1 cm path length quartz cuvette (Starna) and monitored as a function of wavelength. The fluorescence spectra were corrected for the wavelength dependence of the detection system response using the correction curve provided by the manufacturer. The fluorescence spectra were scaled by the absorptance at the excitation wavelength.

KRM Modeling. The experimental absorption and CD spectra were simultaneously fitted with theoretical spectra via a Holstein-like Hamiltonian (Section S8). Due to a larger subpopulation of the optical monomer in the **SQ-Sl$_5$** transverse dimer, which was evident from the fluorescence suppression, the absorption and CD spectra for modeling the **SQ-Sl$_5$** transverse dimer were recorded at 5 °C in order to complete aggregation. The minimum allowed distance between transition dipole moments was restricted to 3.4 Å (whose choice was guided by the van der Waals radius of carbon 1.7 Å doubled and a distance of the $\pi-\pi$ stacking of 3.35 Å). The extended dipole approximation when two point charges of opposite sign are separated by a chromophore length was employed. To account for the potential influence of the DNA environment on covalently linked dyes, the transition dipole moment of the monomer squaraine dye is extracted from modeling experimental absorption of a single dye attached to DNA HJ, that is, the monomer. The characteristic excitonic hopping parameter constant J_0 is derived from the monomer transition dipole moment. The excitonic hopping parameter $J_{m,n}$ is equal to J_0 times a geometrical factor that depends on the distance and orientation of dyes m and n, and that has units of inverse volume. Hence, J_0 sets the values of the $J_{m,n}$ and the distances $R_{m,n}$ between dyes when the aggregate geometry is determined by fitting the Frenkel−Holstein model to the absorbance and CD spectra. Deriving the value of J_0 from the monomer transition dipole moment enables a more accurate determination of $J_{m,n}$ and $R_{m,n}$ than can be achieved if J_0 was treated as a fitting parameter.

The weight of the absorption and CD spectra was controlled via five types of weights. The choice of weighs was guided by the insights from a combination of experimental data. For the aggregates with a pronounced CD signal, the weight of the CD was emphasized, while for the aggregates with either weak or no CD signal, the weight of absorption and CD was kept equal. The theoretical spectra were generated for the theoretical dye configurations found via stochastic gradient search. The goodness of fit was accessed by the several goodness fit parameters (Section S8). The positions of dye transition dipole moments within an aggregate were extracted from the best fit in terms of Cartesian coordinates and zenith and azimuthal angles.

Density Functional Theory Calculations. Solvation energies were determined via DFT calculations as previously described.[63−65] Chemical structures of squaraine dyes were created in Avogadro[66] software, where dye geometries were initially approximated using the universal force field (UFF).[67] Next, the molecular structures in the gas state were optimized using the M06-2X exchange correlation functional[68] and the 6-31+** basis set in Gaussian 16.[69] The implicit continuum solvent model density (SMD)[70] was used for water and *n*-octanol solvents. The solvation energy ΔG was calculated by taking the difference in ground-state energies calculated using SMD water and vacuum given as

$$\Delta G = E_{solv} - E_v$$

where E_{solv} is the ground-state energy calculated in a solvent and E_v is the vacuum or gas-phase ground-state energy.

RESULTS

Molecular Design. Six indolenine squaraine dyes with varying numbers and structures of side substituents were chosen to systematically investigate the influence of hydrophobicity on the excitonic coupling and delocalization in squaraine molecular aggregates covalently templated by DNA HJ. The hydrophobicity of the unsubstituted **SQ-H$_2$** was alternated via disubstitution of the indolenine rings at the 5- and 5′-positions with chloro, methyl, and sulfo groups to afford

https://doi.org/10.1021/acs.jpcc.1c08981
J. Phys. Chem. C 2022, 126, 3475−3488

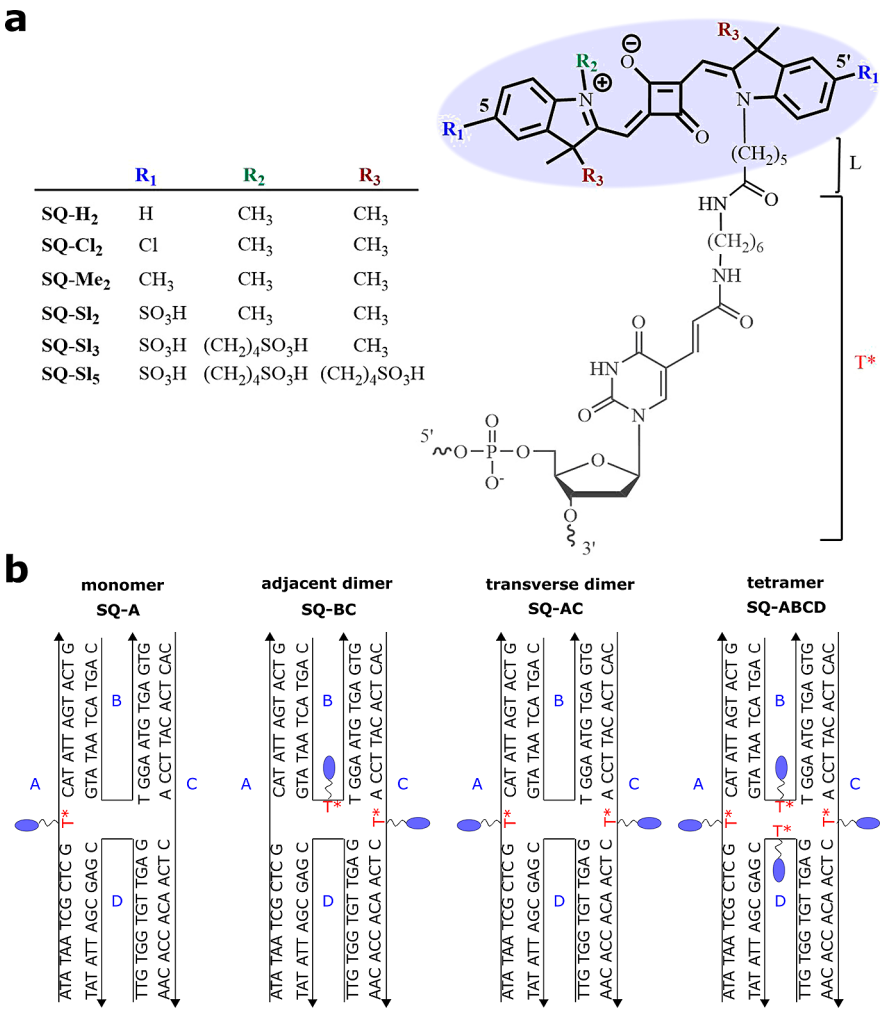

Figure 1. (a) Chemical structures of indolenine squaraine (bold) attached to C6 thymine sequence modifier T*(gray). (b) Schematic representation of immobile four-arm DNA HJs templating squaraine monomer **SQ-A**, adjacent dimer **SQ-BC**, transverse dimer **SQ-AC**, and a tetramer **SQ-ABCD**. The strands comprising DNA HJ are labeled A, B, C and D.

SQ-Cl_2, **SQ-Me_2**, and **SQ-Sl_2**, respectively (Figure 1a). Furthermore, the indolenine nitrogen in **SQ-Sl_2** was substituted with a *N*-sulfobutyl chain to afford **SQ-Sl_3**, which in turn was equipped with two sulfobutyl chains attached to the tertiary carbons of indolenine rings to afford **SQ-Sl_5**. All squaraines were functionalized with the *N*-pentyl-NHS ester for attachment to oligonucleotides. The synthesis of the NHS-ester squaraines is reported in Section S1.

To promote aggregation of squaraines tethered to DNA, we utilized the same immobile DNA HJ template employed previously to create aggregates of a commercially available indolenine squaraine.[54] The *N*-pentyl-NHS ester squaraines were covalently attached to 26-bp oligonucleotides via esterification reactions with the amino C6 thymine sequence modifier (T*) placed in the center of oligonucleotides (Section S1). As a result, the core of a squaraine dye was tethered to the DNA backbone via a single flexible linker constituting the *N*-pentyl fragment "L" of squaraine and the aliphatic fragment of T*(Figure 1a), with an overall length, if fully extended, of about 2.1 nm. Four non-homologous oligonucleotide strands A, B, C, and D were combined in solution to form an immobile 4-arm HJ (Figure 1b). A reference squaraine monomer **SQ-A** was formed by combining squaraine-labeled strand A with unlabeled strands B, C, and D. In a similar manner, SQ-labeled partially complementary strands B and C or non-complementary strands A and C were combined with the corresponding unlabeled strands to create an adjacent **SQ-BC** dimer and a transverse **SQ-AC** dimer, respectively. The tetramer was formed by combining all four SQ-labeled oligonucleotides. To ensure DNA HJ self-assembly, oligonucleotide strands were annealed at 95 °C for 4 min, followed by slow cooling to room temperature. The 1× TBE buffer solution was supplemented with 15 mM $MgCl_2$ to promote a stacked conformation of the DNA HJ. The stacked conformation of DNA HJ in the presence of $MgCl_2$ was observed previously for the analogous DNA HJ templating of commercially available indolenine-based squaraine aggregates.[54] The formation of squaraine aggregates was assessed by analytical non-denaturing polyacrylamide gel electrophoresis. The gel imaging indicated well-formed squaraine-labeled DNA HJs (Section S2, Figure S1).

Relative hydrophobicity of custom squaraines was evaluated via their partitioning between *n*-octanol and water in terms of log $P_{o/w}$. The log $P_{o/w}$ was calculated following eq 2

$$\log P_{o/w} = -\frac{(\Delta G_o - \Delta G_w)}{2.3RT} \quad (2)$$

https://doi.org/10.1021/acs.jpcc.1c08981
J. Phys. Chem. C 2022, 126, 3475−3488

where ΔG_o is the solvation energy in *n*-octanol and ΔG_w is the solvation energy in water, R = 8.31 J*mol^{-1} K^{-1}, and T = 273.15 K. The values of ΔG_o and ΔG_w were obtained via DFT calculations as previously described.[63,64] The more positive log $P_{o/w}$ ($\Delta G_o < \Delta G_w$) is, the more hydrophobic the dye is. Conversely, the more negative log $P_{o/w}$ ($\Delta G_o > \Delta G_w$) is, the greater the propensity of the dyes to be soluble in water, and the more hydrophilic the dye is.

The values of log $P_{o/w}$ were determined for dye structures without a linker and for the dye structures containing a pentyl fragment of the linker denoted as "L" in Figure 1a and Table 1.

Table 1. Squaraine Solvation Energy in Water and *n*-Octanol and log $P_{o/w}$

free dye	ΔG_w, kJ/mol	ΔG_o, kJ/mol	log $P_{o/w}$
SQ-Cl$_2$	−82.2	−110	5.31
SQ-H$_2$	−79.3	−102	4.30
SQ-Me$_2$	−76.5	−104	5.24
SQ-Sl$_2$	−181	−161	−3.66
SQ-Sl$_3$	−244	−211	−6.26
SQ-Sl$_5$	−320	−258	−11.82
SQ-Me$_2$-L	−73.4	−136	11.94
SQ-Cl$_2$-L	−77.8	−116	7.33
SQ-H$_2$-L	−75.5	−108	6.26
SQ-Sl$_2$-L	−176	−170	−1.07
SQ-Sl$_3$-L	−236	−215	−3.97
SQ-Sl$_5$-L	−304	−290	−2.75

Based on the obtained values of log $P_{o/w}$ (Table 1), custom squaraines were divided into two groups: overall hydrophobic squaraines **SQ-H$_2$**, **SQ-Cl$_2$**, and **SQ-Me$_2$** (log $P_{o/w} > 0$) and overall hydrophilic squaraines **SQ-Sl$_2$**, **SQ-Sl$_3$**, and **SQ-Sl$_5$** (log $P_{o/w} < 0$). When not accounting for the contribution of the linker, the hydrophobic dyes **SQ-H$_2$**, **SQ-Cl$_2$**, and **SQ-Me$_2$** exhibited comparable hydrophobicity in terms of log $P_{o/w}$ being in the range 4.30−5.31. With the linker, the difference in hydrophobicity of **SQ-H$_2$**, **SQ-Cl$_2$**, and **SQ-Me$_2$** became more apparent increasing in the order of **SQ-H$_2$-L** < **SQ-Cl$_2$-L** < **SQ-Me$_2$-L**. The hydrophobicity of hydrophilic squaraines without contribution of the linker increased in order **SQ-Sl$_5$** < **SQ-Sl$_3$** < **SQ-Sl$_2$**, which is in accordance with the experimental aqueous solubilities previously observed for the *N*-pentylcarboxy derivatives of **SQ-Sl$_5$** and **SQ-Sl$_2$** dyes in phosphate buffer.[62] Inclusion of the linker strongly increased hydrophobicity of **SQ-Sl$_3$-L** and **SQ-Sl$_5$-L** and resulted in the hydrophobicity order **SQ-Sl$_3$-L** < **SQ-Sl$_5$-L** < **SQ-Sl$_2$-L**.

Thermal Denaturation. To characterize overall stabilities of DNA HJs templating transverse and adjacent squaraine dimers, we performed thermal denaturation experiments. The melting temperature of the unlabeled DNA HJ was used as a reference control (T_m = 60.0 °C).[54] With the exception of the **SQ-H$_2$** transverse dimer, both adjacent and transverse dimers of hydrophobic dyes melted at a higher temperature than unlabeled HJ, indicative of dye−dye interactions having an overall stabilizing effect on the DNA−dye construct. In contrast, dimers of hydrophilic dyes melted at a lower temperature than unlabeled HJ. The HJs templating **SQ-Cl$_2$** dimers were characterized by the highest melting points. Notably, the melting temperatures of HJs increased as dye hydrophobicity increased (Section S3). As such, a hydrophobic effect can be considered as a major contributor of aggregation of dyes covalently templated by DNA.

Steady-State Optical Characterization. First, the squaraine monomers, as reference samples, were examined via steady-state absorption, emission, and circular dichroism (CD) spectroscopies (Figure 2 and 3, Sections S4−S7). All squaraine monomers covalently attached to DNA HJ exhibited electronic absorption spectra characteristic of the squaraine dye family. Both hydrophilic and hydrophobic squaraines templated via DNA HJs exhibited extinction coefficient values similar to those of the corresponding free dyes. However, hydrophobic squaraines were characterized with slightly lower extinction coefficient values (257,000−264,000 M^{-1} cm^{-1}) compared to those of hydrophilic squaraines containing sulfo groups (282,000−304,000 M^{-1} cm^{-1}). The attachment of hydrophobic **SQ-Cl$_2$**, **SQ-Me$_2$**, and **SQ-H$_2$** to DNA HJ resulted in a 10−13 nm red shift of their absorption maxima compared with those of free dyes (Table 2). A similar spectral shift of 9 nm observed previously for free dyes **SQ-H$_2$** and **SQ-Cl$_2$** upon transitioning from polar methanol to nonpolar dichloromethane was attributed to the solvatochromic effect.[62] In our case, the red shift is likely to be caused by the squaraine being located around hydrophobic DNA. Squaraines containing sulfo groups also showed a red shift of absorption maxima upon attachment to DNA. While for **SQ-Sl$_2$**, the red shift was 12 nm and comparable with the red shift of hydrophobic squaraines, **SQ-Sl$_3$** and **SQ-Sl$_5$** were only red-shifted 5 and 3 nm, respectively. Squaraines **SQ-Sl$_2$**, **SQ-Sl$_3$**, and **SQ-Sl$_5$** have been previously covalently attached to the IgG antibody,[62] and exhibited small red shifts of 6, 5, and 4 nm, respectively, observed upon transitioning from an aqueous environment to a less-polar protein environment. Based on this comparison and chemical structures, non-covalent binding with DNA is less likely for hydrophilic and bulkier dyes **SQ-Sl$_3$** and **SQ-Sl$_5$**.

The squaraine monomers exhibited strong fluorescence emission as a near mirror image of absorption with clear (0−0) and (0−1) emission transitions, and small Stokes shifts in the range of 24−39 meV or 194−315 cm^{-1} (Figure S5 and Table S2). No specific correlation between substituents and Stokes shifts was observed indicating that the introduction of the side substituents does not noticeably affect the rigidity of the indolenine squaraine core.

In the CD spectra, all constructs exhibited a well-defined couplet in the 260−280 nm region indicative of a well-formed duplex DNA (Section S7). Because squaraine dyes are achiral, they are not expected to produce a CD signal in the visible region. Each monomer of **SQ-H$_2$**, **SQ-Me$_2$**, **SQ-Sl$_2$**, **SQ-Sl$_3$**, and **SQ-Sl$_5$** did not induce a signal in the visible region of the CD spectra. However, the monomers of **SQ-H$_2$** and **SQ-Cl$_2$** exhibited a very weak induced CD signal, which indicates that these dyes may interact with DNA by intercalating between base pairs or binding to the minor or major groove resulting in restriction of their conformational freedom and induced chirality.

The aggregation ability of hydrophilic and hydrophobic squaraine aggregates covalently attached to the DNA HJ was evaluated by steady-state absorption, emission, and CD spectroscopies, and compared within the adjacent dimer, transverse dimer, and tetramer series.

Hydrophilic squaraines exhibited noticeable spectral changes in dimer configurations with respect to their monomers (Figure 2 and Table 2). The spectral changes included (1) a blue shift of both low- and high-energy absorption bands that we, respectively, assign as A_1 and A_2; and (2) intensification of the A_2 band with the suppression of the A_1 band, that is, an

https://doi.org/10.1021/acs.jpcc.1c08981
J. Phys. Chem. C 2022, 126, 3475−3488

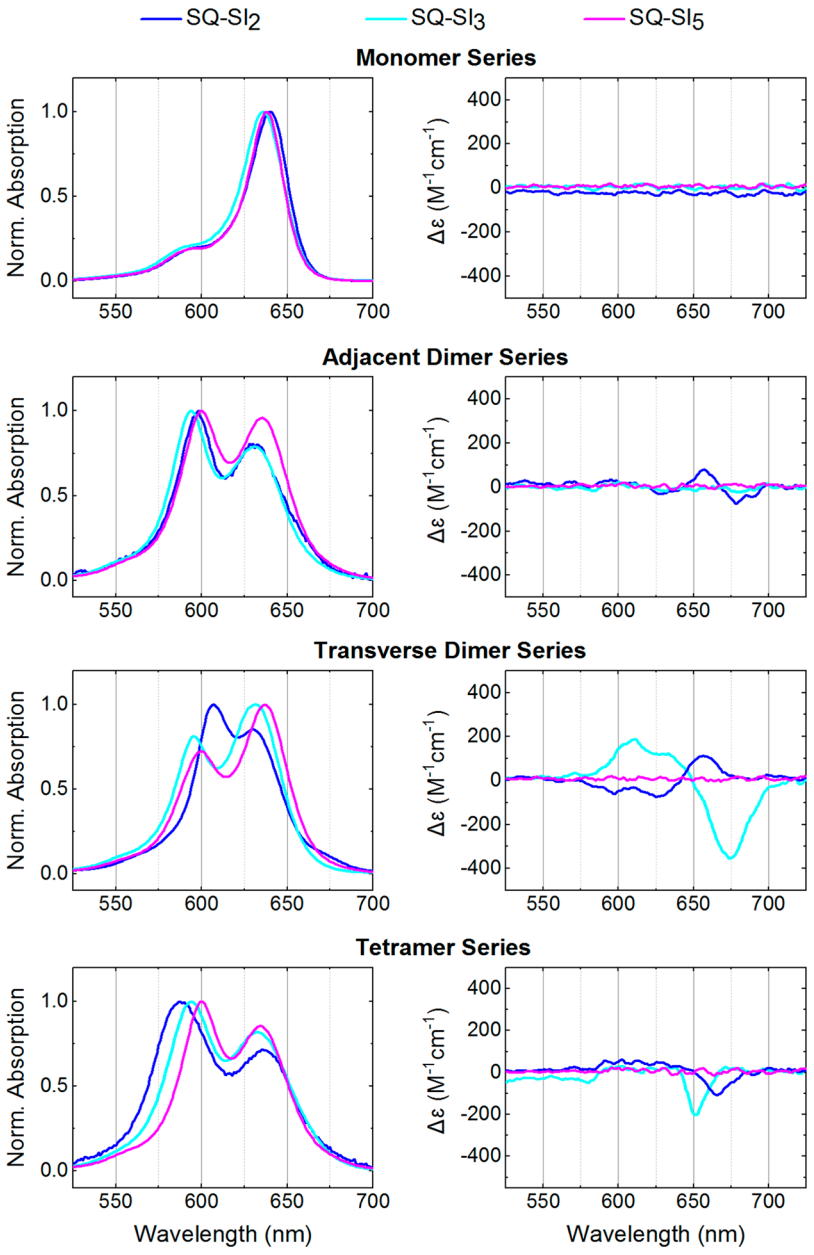

Figure 2. (Left column) Acquired steady-state absorption spectra normalized at the dye peak maximum of the hydrophilic squaraine-DNA constructs in 1× TBE, 15 mM $MgCl_2$ at room temperature. (right column) Acquired CD of the hydrophilic squaraine-DNA constructs in 1× TBE, 15 mM $MgCl_2$ at room temperature. The squaraine-DNA construct concentration was 1.5 μM.

increase of the A_2/A_1 ratio. The blue shift for adjacent and transverse dimers increased in the order of **SQ-SI$_5$** < **SQ-SI$_2$** < **SQ-SI$_3$**. Both dimers of **SQ-SI$_2$** and adjacent dimers of **SQ-SI$_3$** and **SQ-SI$_5$** exhibited a more intense high-energy band (A_2 > A_1), while transverse dimers **SQ-SI$_5$** and **SQ-SI$_3$** had more intense low-energy band (A_2 < A_1). In accordance with the Kasha's exciton theory,[11,71] these spectral changes indicate that hydrophilic squaraines covalently attached to DNA HJ formed dimer aggregates with the spectral signatures of excitonic coupling and delocalization. This observation was not anticipated especially for **SQ-SI$_3$** and **SQ-SI$_5$** as these dyes in free form were shown not to aggregate at concentrations of 0.2 and 6 mM, respectively, in aqueous solution.[62] The blue shift in the dimers of hydrophilic squaraines is consistent with a face-to-face orientation of transition dipole moments, that is, a H-aggregate, while similar intensities of A_1 and A_2 bands indicate the involvement of vibronic coupling[11,71] and the overall intermediate coupling regime.[11] The adjacent and transverse dimers of hydrophilic squaraines were also characterized by CD spectroscopy (Figure 2 (right column)). Achiral **SQ-SI$_2$** and **SQ-SI$_3$** dyes exhibited an exciton-induced bisignate CD signal in their transverse and adjacent dimers indicating on a chiral orientation of transition dipole moments in the aggregates. Though the CD signal originates from chirality of optical system, the absence of chirality does not necessarily mean a lack of excitonically coupled transition dipole moments (TDM), but might be attributed to an aggregate having a mirror plane in the orientation of transition dipole moments. This situation takes place when transition dipole moments are coplanar, which might be the case for the **SQ-SI$_3$** transverse dimer and **SQ-SI$_5$** dimers.

https://doi.org/10.1021/acs.jpcc.1c08981
J. Phys. Chem. C 2022, 126, 3475−3488

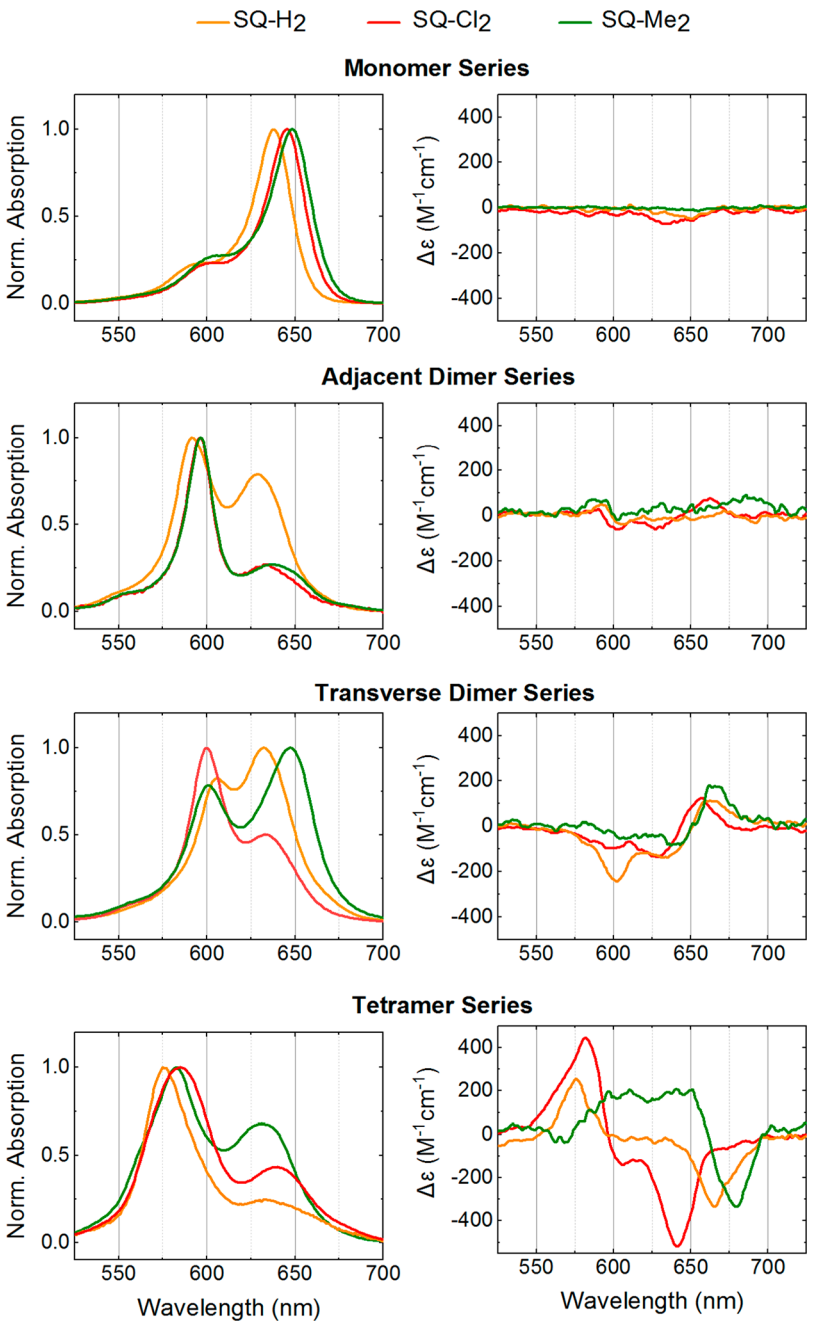

Figure 3. (Left column) Acquired steady-state absorption spectra normalized at the dye peak maximum of the hydrophobic squaraine-DNA constructs in 1× TBE, 15 mM $MgCl_2$ at room temperature. (right column) Acquired CD of the hydrophobic squaraine-DNA constructs in 1× TBE, 15 mM $MgCl_2$ at room temperature. The squaraine-DNA construct concentration was 1.5 μM.

Upon dimer assembly via DNA HJ, hydrophobic squaraines demonstrated profound spectral changes evident in a blue shift and in an increase of the A_2/A_1 absorption band ratio with respect to the monomers (Figure 3, Table 2). The blue shift of the high A_2 and low A_1 energy bands increased in the order of **SQ-H$_2$** < **SQ-Me$_2$** < **SQ-Cl$_2$**, and for each dye the shift was larger in the adjacent dimer than in the transverse dimer. The A_2/A_1 ratio increased in the order of **SQ-H$_2$** < **SQ-Me$_2$** ≤ **SQ-Cl$_2$**, where A_2 was greater than A_1 for all hydrophobic squaraine adjacent dimers and for the **SQ-Cl$_2$** transverse dimer. For the transverse dimers of **SQ-H$_2$** and **SQ-Me$_2$**, A_2 was smaller than A_1. Evident from these changes, all hydrophobic squaraines formed H-type dimers with increasing excitonic coupling strengths as the hydrophobicity increases. Thus, the two most hydrophobic squaraines—**SQ-Cl$_2$** and **SQ-Me$_2$**—appeared to exhibit the strongest excitonic coupling based on the blue shift, as well as nearly complete suppression of the low-energy band A_1 (Tables 2 and 3). While adjacent dimers of **SQ-Cl$_2$** and **SQ-Me$_2$** showed nearly identical spectral shapes, the peak extinction coefficient of the high-energy absorption band A_2 of **SQ-Cl$_2$** was considerably larger than that of **SQ-Me$_2$** (Figure S4). Overall, the magnitude of excitonic coupling estimated from spectral profiles closely follows the order of relative hydrophobicity of hydrophobic squaraines. Although both adjacent and transverse dimers show signatures of excitonic coupling and delocalization, such signatures are

https://doi.org/10.1021/acs.jpcc.1c08981
J. Phys. Chem. C 2022, 126, 3475−3488

Table 2. Experimental Absorption Properties of Squaraines and Squaraine Aggregate Template via DNA HJ

	absorption peak maximum, nm				
dye	[a]free dye	[d]HJ monomer	[d]trans dimer	[d]adj dimer	[d]tetramer
SQ-H$_2$	[b]628	638	606; 632	592; 629	583; 631
SQ-Cl$_2$	[b]633	645	600; 633	596; 633	575; 633
SQ-Me$_2$	[b]635	648	602; 647	596; 637	583; 640
SQ-Sl$_2$	628	640	607; 630	598; 630	587; 635
SQ-Sl$_3$	[c]631	636	596; 632	594; 631	594; 633
SQ-Sl$_5$	[c]636	638	602; 637	600; 636	600; 634

[a]As carboxylic acid in phosphate buffer, pH = 7.4. [b]In methanol. [c]From [ref. 29]. [d]Measurements were carried out in 1× TBE, 15 mM $MgCl_2$ containing 1.5 μM DNA construct at room temperature.

Table 3. Spectral Characteristics of Squaraine Aggregates

	adj dimer		trans dimer		tetramer	
dye	[a]A_2/A_1	[b]FS, %	A_2/A_1	FS, %	A_2/A_1	FS, %
SQ-H$_2$	1.26	90.5	0.82	83.8	1.48	95.8
SQ-Cl$_2$	3.72	92.6	1.99	90.4	4.06	96.9
SQ-Me$_2$	3.70	84.8	0.78	75.1	2.33	95.5
SQ-Sl$_2$	1.24	87.3	1.17	87.3	1.41	95.4
SQ-Sl$_3$	1.27	69.5	0.81	74.7	1.22	88.1
SQ-Sl$_5$	1.04	78.7	0.72	48.4	1.17	87.1

[a]A_1 and A_2 are relative intensities of low-energy and high-energy absorption bands in the absorption spectra of squaraine dimers recorded at a 1.5 μM dye-DNA concentration in 1× TBE, 15 mM $MgCl_2$. [b]FS is fluorescence suppression.

apparently diminished for the hydrophobic dyes in the transverse dimer configuration suggesting weaker excitonic coupling and more oblique aggregates. The difference in the absorption properties between transverse and adjacent dimers suggests that the adjacent configuration of dye attachment is more favorable for promoting strong excitonic coupling in indolenine squaraine-based dimer aggregates. The exciton-induced CD spectra of hydrophobic squaraines (Figure 3, right) further supported the formation of dimer aggregates.

Fluorescence emission measurements were performed to gain insights on the structure and dynamics of the squaraine dimer excited states (Tables 3 and S2). The fluorescence from the squaraine dimer solutions occurred approximately at the same wavelength as the fluorescence of the corresponding monomer solutions; however, the intensity of aggregate fluorescence was strongly suppressed (Table 3). A similar fluorescence behavior between monomer and dimer emission was previously observed for the dimers of commercial indolenine squaraines, and was assigned to the presence of optical monomers, that is, a subpopulation of dyes attached to DNA in pairs, but not forming an aggregate.[50] Based on our experimental observations and the preceding study, we assign the observed emission in dimer samples to the strongly emissive optical monomers. The emission from the dimers may still occur, but it would be very weak and not measurable for the following reasons. According to the selection rules in the Kasha's theory on the molecular aggregates,[11] the radiative decay, that is, fluorescence, is prohibited from the high excited state in the H-aggregates. Moreover, strong fluorescence quenching in dye aggregates has been recently associated with the new non-radiative decay pathways available in strongly coupled aggregates.[32,50,53,72] Thus, the extent of fluorescence suppression (FS), calculated in Table 3, can provide insights, at least qualitatively, into the strength of excitonic coupling (i.e., "weak" or "strong") between dyes in squaraine dimers and the presence of subpopulation of optical isomers. The strongest FS of >90% was observed for the dimers of **SQ-Cl$_2$** suggesting a strong excitonic coupling. Other dimers (with the exception of transverse dimer **SQ-Sl$_5$**) exhibited smaller FS in the range of 70−87%. The dimers of hydrophobic dyes **SQ-H$_2$**, **SQ-Cl$_2$**, and **SQ-Me$_2$** exhibited stronger FS in the adjacent configuration than in the transverse configuration. In contrast, the hydrophilic dyes **SQ-Sl$_2$** and **SQ-Sl$_3$** showed stronger FS in the transverse configuration. While the fluorescence in the **SQ-Sl$_5$** adjacent dimer was suppressed by 79% and similarly to other adjacent dimers, the **SQ-Sl$_5$** transverse dimer exhibited significantly smaller FS of 48% indicative of a larger subpopulation of **SQ-Sl$_5$** optical monomers. Note that electrophoretic analysis (Figure S1) showed a minor amount (and comparable to other squaraine dimers) of unhybridized single strand labeled with **SQ-Sl$_5$**, suggesting that the observed fluorescence emission of the **SQ-Sl$_5$** transverse dimer sample should not be attributed to the **SQ-Sl$_5$** monomer attached to a single strand in solution.

One of the special features of the DNA HJ as a template is that it allows one to create dye tetramers. Upon tetramer formation, pronounced spectral changes were observed for all hydrophobic dyes **SQ-Cl$_2$**, **SQ-Me$_2$**, and **SQ-H$_2$** and a hydrophilic **SQ-Sl$_2$** indicative of the strong excitonic coupling and delocalization among the four dyes (Figures 2 and 3, Table 2 and 3). In particular, the high-energy band carrying the most oscillator strength was further blue-shifted by 613 cm^{-1} for **SQ-Cl$_2$**, 374 cm^{-1} for **SQ-Me$_2$**, 313 cm^{-1} for **SQ-Sl$_2$**, and 261 cm^{-1} for **SQ-H$_2$** with respect to the corresponding high-energy band A_2 in adjacent dimers. These changes in absorption, as compared to the monomer absorption, indicated the H-type packing of these dyes in the tetramer configuration. The CD spectra of tetramers were characterized by intense exciton-induced couplets (Figures 2 and 3). Moreover, the fluorescence was nearly quantitatively suppressed (96% on average) in the tetramers of **SQ-H$_2$**, **SQ-Cl$_2$**, **SQ-Me$_2$**, and **SQ-Sl$_2$**. In contrast, hydrophilic **SQ-Sl$_3$** and **SQ-Sl$_5$** squaraines did not demonstrate strong evidence of tetramer formation. The absorption peak maximum of **SQ-Sl$_3$** and **SQ-Sl$_5$** did not shift, while the absorbance extinction was almost doubled compared to their adjacent dimers (Figure S4). The FS in **SQ-Sl$_3$** and **SQ-Sl$_5$** tetramers appeared to be comparable with one observed in their adjacent dimers. Collectively, these observations indicate that **SQ-Sl$_3$** and **SQ-Sl$_5$** might mostly remain in their dimer form. The steric bulkiness of **SQ-Sl$_3$** and **SQ-Sl$_5$** may interfere with dye aggregation and/or the DNA HJ template, thus inhibiting the formation of **SQ-Sl$_3$** and **SQ-Sl$_5$** tetramers.

Theoretical Spectral Modeling. The modeling approach developed in our group, based on the theoretical approach of Kühn−Renger−May (KRM),[73] has been demonstrated to be a powerful tool in extracting excitonic hopping parameter $J_{m,n}$ as a quantitative metric of excitonic coupling strength, as well as the geometric parameters of the dye aggregates.[51,52,54] The advantage of KRM modeling of dye aggregates stems from considering not only electronic contribution of dyes to the excitonic coupling but also their vibronic contribution. The vibronic contribution is considered via the dominant vibrational mode of each dye, which for squaraines has an energy of ca. 0.12−0.17 meV (970−1400 cm^{-1}). To model Coulomb

https://doi.org/10.1021/acs.jpcc.1c08981
J. Phys. Chem. C 2022, 126, 3475−3488

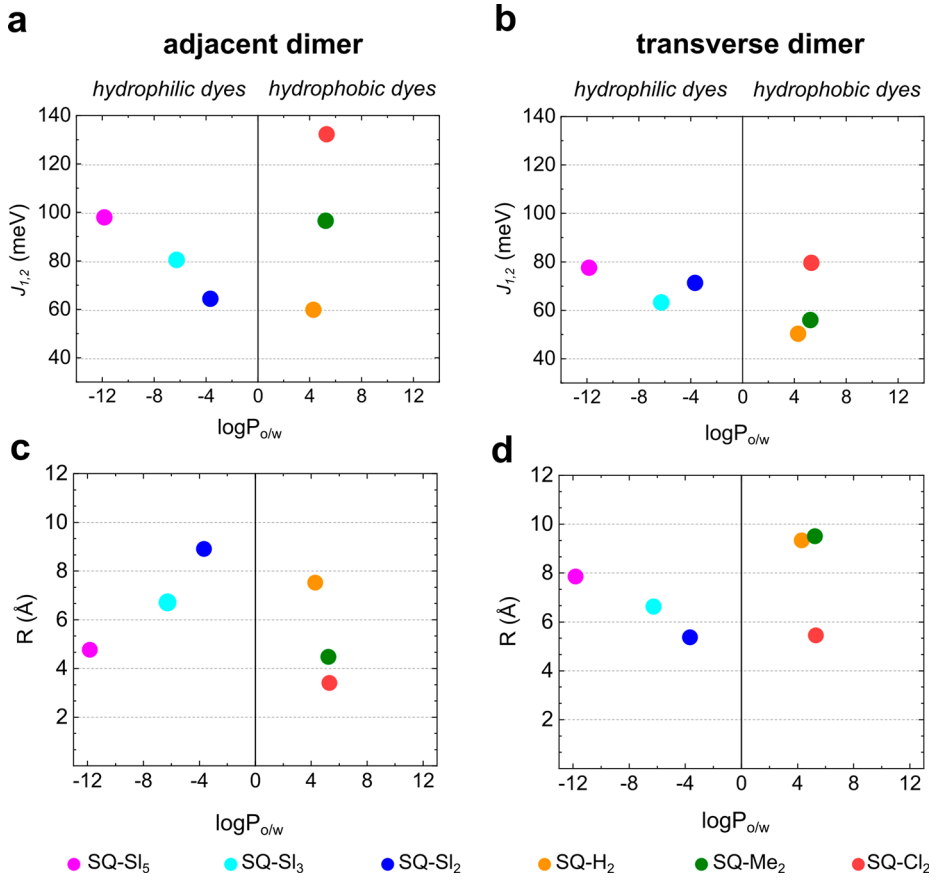

Figure 4. (a,b) KRM values of $J_{1,2}$ in adjacent and transverse squaraine dimers plotted against squaraine partitioning between *n*-octanol and water (no linker included). (c,d) KRM values of center-to-center distance *R* in Å in adjacent and transverse squaraine dimers plotted against squaraine partitioning between *n*-octanol and water (no linker included).

interaction between squaraines, we employed an extended dipole approximation,[74] where the dipoles were modeled as two point charges of opposite sign and equal magnitude separated by nearly the dye length. This extended dipole approximation is particularly beneficial when dye intermolecular distances are much shorter than the dye length as this approach better accounts for the charge distribution over a large molecule.

From the KRM modeling results, we extracted excitonic hopping parameter $J_{1,2}$ for each dimer and for each dye pair in a tetramer. Squaraine dimers exhibited medium to strong excitonic hopping parameter $J_{1,2}$ ranging from 50.3 meV (406 cm^{-1}) to 132.2 meV (1065 cm^{-1}) with the strongest $J_{1,2}$ observed in the **SQ-Cl$_2$** adjacent dimer. For comparison, the excitonic coupling in analogous dimers of the commercial squaraine and cyanine dyes Square 660 and Cy5 were estimated to be 65−68 and 70 meV, respectively. Michail et al. reported very similar coupling strengths (from 930 cm^{-1} or 118 meV to 390 cm^{-1} or 48 meV) in the J-aggregates of indolenine squaraine dimers, where squaraine molecules were linked via a covalent bridge of varying lengths.[75] The extracted $J_{1,2}$ values were plotted against dye partitioning between water and *n*-octanol as a measure of dye hydrophobicity (Figure 4a,b). A general trend was evident for the hydrophobic squaraines **SQ-H$_2$**, **SQ-Cl$_2$**, and **SQ-Me$_2$** in both adjacent and transverse dimer series, where $J_{1,2}$ generally increased as hydrophobicity increased. Hydrophilic squaraines containing sulfo groups showed an opposite trend: a decrease in $J_{1,2}$ upon an increase in partitioning. Squaraine **SQ-Sl$_5$**, being the most hydrophilic dye, exhibited the excitonic coupling comparable to and exceeding the coupling of more hydrophobic dyes especially in the adjacent dimer configuration. Plotting partitioning accounting for the linker fragment versus $J_{1,2}$ (Figure S13) resulted in the same general trends as those without linker contribution (Figure 4), with the exception of **SQ-Sl$_5$** and **SQ-Cl$_2$**. To evaluate the role of hydrophobicity in the strength of excitonic coupling in squaraine tetramers, the highest value of $J_{m,n}$ and the arithmetic mean $J_{m,n\text{ave}}$ for each squaraine tetramer was plotted against the partitioning between *n*-octanol and water with (Figure S13c) and without the linker fragment of that squaraine (Figure 5). With the linker contribution, an apparent trend was observed between excitonic coupling in the tetramer and dye hydrophobicity (Figures 5 and S13c). **SQ-Sl$_3$** and **SQ-Sl$_5$** were excluded from the KRM modeling as tetramers because steady-state spectroscopy did not indicate the formation of tetramers with these dyes. The absence of a reliable trend between partitioning and $J_{m,n}$ indicates that effects other than hydrophobic effect influence the strength of excitonic coupling in squaraine aggregates. Among those effects are steric hindrance and electrostatic forces of various origin that we evaluated in Section S9.

The geometry of squaraine dimers (Table 4) and tetramers (Tables S10−S13) was characterized by several geometric parameters derived from KRM modeling: (1) a center-to-center distance R between two TDMs, (2) the shortest distance d between TDMs, (3) oblique angle α as a quantitative measure of deviation from the parallel stacking

https://doi.org/10.1021/acs.jpcc.1c08981
J. Phys. Chem. C 2022, 126, 3475−3488

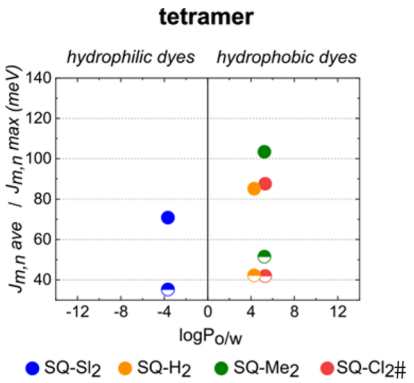

Figure 5. KRM values of the highest $J_{m,n}$ value (solid circles) and $J_{m,n\text{ave}}$ (half solid circles) in squaraine tetramers plotted against partitioning between *n*-octanol and water as a measure of hydrophobicity (no linker included).

of TDMs (α = 0°), and (4) a slip angle θ_s as a measure of sliding or displacement of one dye relative to another along dye's TMD (when θ_s = 90°, the dyes are not displaced) (Table 4 inset). The value of *R* is useful, as we expect smaller *R* to result in an increased excitonic coupling strength (and which we expect to decrease for increasingly hydrophobic dyes).[11] Among hydrophobic squaraines, *R* values decreased as the dye hydrophobicity increased (Figure 4c,d). Among the six squaraines, the values of *R* varied on the Angstrom level in the range from 3.4 to 9.5 Å. The hydrophobic squaraines generally exhibited smaller *R* in the adjacent dimer configuration, which is more favorable for the excitonic coupling in aggregates of these dyes. As expected, the most hydrophobic **SQ-Cl$_2$** has the smallest R in both adjacent and transverse dimers. Counterintuitively, the most hydrophilic **SQ-Sl$_5$** exhibited the smallest *R* among the hydrophilic squaraines. The value of α was used to characterize the amount of obliqueness with two extreme cases being α = 0°, that is, parallel TDMs and α = 90°, that is, a purely oblique dimer. In general, transverse dimers of squaraines were more oblique than adjacent dimers of analogous dyes. Adjacent dimers of **SQ-Cl$_2$** and **SQ-Me$_2$** showed nearly parallel alignment of their TDMs (Figure S10) and thereof indolenine rings were characterized by α in the range 1.35−2.4°, but differed in the slip angle or displacement. In particular, dyes in the **SQ-Cl$_2$** adjacent dimer were barely displaced (θ_s = 86.8°), while dyes in the **SQ-Me$_2$** dimer were noticeably displaced relative to each other (θ_s = 59.0°). The KRM modeling predicts the shortest distance d for the most dimers to be 3.4−3.8 Å. At this distance, molecules containing π-bond networks are known to undergo strong $\pi-\pi$ interactions.[76] The adjacent dimer of **SQ-Cl$_2$** is the only dimer, where the $\pi-\pi$ interactions between indolenine rings can take place on both ends of the dimer based on a center-to-center distance of 3.4 Å and parallel orientation of TDMs.

DISCUSSION

Three overall hydrophobic squaraine dyes with varying hydrophobicity, covalently tethered to and templated via DNA HJ, formed dimer and tetramer aggregates as was evident via drastic changes in their optical properties compared to their respective monomers. These results are in accordance with prior reports on aggregation of various dye families including cyanine dyes, where the hydrophobic effect was identified as a major driving force in both spontaneous aggregation,[55−61] and aggregation via non-covalent DNA-templating in aqueous solution.[23] The focus of those studies, however, was a general dye propensity toward aggregation, that is, the ability to form dimers and multimers and the associated equilibrium constants. In the work most relevant to the present study, Armitage and co-workers templated aggregates of a series four hydrophobic cyanine dyes[23] via non-covalent binding to DNA. In that work, the excitonic coupling strength was estimated as twice the difference in energy between the monomer and dimer UV−Vis absorbance bands. While the study demonstrated that hydrophobic dyes tend to form aggregates with strong excitonic coupling, it was unable to provide any further insight into how a chemical structure impacts hydrophobicity, strength of excitonic coupling, and aggregate geometry parameters such as the intermolecular distance and relative orientation of dyes. In the present work, we used a combination of DFT, KRM modeling, and melting experiments to gain additional insights into correlations between the chemical structure, extent of hydrophobicity, strength of

Table 4. Geometric Parameters Derived by KRM Modeling of the Optical Properties of Adjacent and Transverse Dimer Aggregates[a]

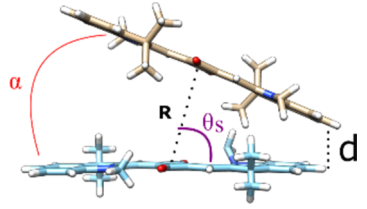

	adjacent dimer					transverse dimer				
dye	$J_{1,2}$, meV	*R*, Å	θ_s, deg	α, deg	d, Å	$J_{1,2}$, meV	*R*, Å	θ_s, deg	α, deg	*d*, Å
SQ-Cl$_2$	132.2	3.40	86.8	1.35	3.4	79.6	5.45	81.8	15.7	3.5
SQ-Me$_2$	96.5	4.47	59.0	2.4	3.6	55.9	9.5	74.9	55.5	3.4
SQ-H$_2$	59.8	7.52	64.8	32.7	3.4	50.3	9.33	74.8	47.5	3.5
SQ-Sl$_2$	64.3	8.9	75.0	48.3	3.6	71.3	5.4	60.0	8.8	4.0
SQ-Sl$_3$	80.4	6.71	71.0	25.8	3.4	63.2	6.62	71.3	19.8	3.8
SQ-Sl$_5$	97.9	4.76	89.2	9.0	3.6	77.5[a]	7.85	69.3	34.6	3.4

[a]Modeling of experimental absorption and CD recorded at 5 °C.

https://doi.org/10.1021/acs.jpcc.1c08981
J. Phys. Chem. C 2022, 126, 3475−3488

excitonic coupling, and intermolecular distance in squaraine aggregates templated by DNA. In line with our expectations, the melting experiments demonstrated that the more hydrophobic squaraines afford more stable HJs templating the squaraine aggregates suggesting a driving effect of hydrophobic forces on the aggregation of squaraines covalently templated by DNA. Moreover, our results revealed that squaraines with a more hydrophobic structure afford a denser packing, or closer intermolecular distances ($R_{m,n}$), in their dimer and tetramer aggregates. A denser packing in aggregates of more hydrophobic squaraines further manifests in larger values of excitonic hopping parameter $J_{m,n}$ in accordance with the Kasha's exciton model (eq 1), where smaller $R_{m,n}$ corresponds to larger $J_{m,n}$. In the present study, the largest value of $J_{m,n}$ was observed for the most hydrophobic squaraine **SQ-Cl$_2$**. In addition, the correlation between hydrophobicity and packing was the most apparent when dyes were attached to partially complementary strands of DNA HJ (adjacent dimer configuration) perhaps because the sites of dye's linker attachment to DNA are closer in space in this configuration than when dyes are attached to non-complementary strands of DNA HJ (the transverse dimer configuration).

Taking advantage of covalent DNA-templating, we were able to evaluate aggregation ability of hydrophilic dyes commonly excluded from the studies on spontaneous dye aggregation and aggregation via non-covalent DNA templating. We found that when covalently templated to DNA, "hydrophilic" dyes can form aggregates, and the excitonic coupling in aggregates of these hydrophilic dyes is comparable with that of hydrophobic dyes. These results appear counterintuitive with regard to Markova's study, where free dyes **SQ-Sl$_2$** and **SQ-Sl$_5$** did not show signs of aggregation at the concentrations of 0.2 and 6 mM, respectively, in aqueous phosphate buffer.[62] We explain this discrepancy with the ability of the DNA template to bring dyes in proximity including water-soluble dyes that otherwise stay in the free form in aqueous solution. We attempt to interpret these results in the context of a conventional understanding of a physical origin of the hydrophobic effect that is thought to be entropy-driven at room temperature.[57,77] In particular, when a hydrophobic surface area is minimized upon aggregation of hydrophobic molecules that are not able to interact with water, the network of water hydrogen bonding with higher entropy is restored. The high entropy of the water structure upon aggregation of hydrophobic molecules compensates the entropy decrease of the aggregated molecules as well as the enthalpic cost of reorganization into an aggregate making the aggregation overall favorable. Conversely, hydrophilic molecules are able to form hydrogen bonds with water, so their aggregation does not afford an increase in water entropy large enough to make the aggregation favorable. However, when hydrophilic dyes are brought in proximity via covalent attachment to DNA, their reorganization into an aggregate occurs readily at a very small energetic cost. When **SQ-Sl$_3$** and **SQ-Sl$_5$** aggregate, the hydrophobic butyl chains of **SQ-Sl$_3$** and **SQ-Sl$_5$** can be involved in hydrophobic interactions in the presence of polar sulfo groups. Squaraines **SQ-Sl$_3$** and **SQ-Sl$_5$** possess the largest surface area among the squaraines in this study (Section S9), which might explain stronger coupling in their aggregates than expected from their overall hydrophilic nature. In this regard, aggregation of DNA-templated hydrophilic dyes can be compared to protein folding, where overall hydrophilic amino acids such as lysine were shown to participate in initial protein folding via hydrophobic interactions between their non-polar alkyl chains.[78]

Factors beyond hydrophobicity, such as dye sterics and electrostatic interactions, may additionally influence dye aggregation. The steric influence becomes apparent in the attempt to aggregate **SQ-Sl$_3$** and **SQ-Sl$_5$** into tetramers. Though sulfobutyl chains appear to be accommodated in the dimers of **SQ-Sl$_3$** and **SQ-Sl$_5$**, their bulkiness strongly hinders the formation of **SQ-Sl$_3$** and **SQ-Sl$_5$** tetramers attached to DNA HJ. We evaluated influence of electrostatic interactions such as dipole−dipole interactions and induced-dipole interactions including dispersion via a static dipole moment and polarizability (Section S9). The results showed that while electrostatic forces do not appear to be major contributors in excitonic coupling, forces involving induced dipoles still play a more apparent role for hydrophobic squaraines. Hydrophobic squaraines **SQ-H$_2$**, **SQ-Me$_2$**, and **SQ-Cl$_2$** have comparable hydrophobicity and surface area, though differ in polarizability. Higher polarizability of **SQ-Cl$_2$** and **SQ-Me$_2$** than that of **SQ-H$_2$** suggests stronger induced-dipole electrostatic forces in the dimers of the former dyes, and may explain the increase in $J_{1,2}$ in adjacent dimers of **SQ-Me$_2$** and **SQ-Cl$_2$** compared to those of **SQ-H$_2$**. Furthermore, having comparable polarizabilities, **SQ-Cl$_2$** dimers exhibit significantly stronger excitonic coupling than dimers of **SQ-Me$_2$**. From the KRM modeling, we found that in the adjacent dimer **SQ-Cl$_2$**, TDMs, and hence the indolenine rings, are parallel and lack the displacement. According to the pioneering model of Hunter and Sanders,[79] the lack of displacement suggests less electrostatic repulsion between the static charge distributions in π-systems and, hence, stronger $\pi-\pi$ interactions stabilizing a dimer. Examination of the electrostatic potential surfaces revealed slightly decreased electron density in the electron-rich indolenine rings of **SQ-Cl$_2$** due to the electron-withdrawing effect of chlorine atoms presumably allowing **SQ-Cl$_2$** to align without displacement (Section S9). In contrast, electron-donating methyl groups slightly increase the electron density of indolenines in **SQ-Me$_2$** leading to the displacement in its dimer. Further insights into how these parameters influence aggregate geometry and excitonic coupling strength may require a similar study specifically targeting a set of dyes tailored to vary steric or electrostatic interactions.

CONCLUSIONS

Six examined indolenine squaraines with varying degrees of hydrophobicity demonstrated aggregate behavior, excitonic coupling, and exciton delocalization when covalently templated as adjacent and transverse dimers by DNA HJ in aqueous buffer. While aggregation of hydrophobic dyes was anticipated, the observed aggregation of hydrophilic dyes was not necessarily expected. The excitonic coupling was evident via spectral changes that indicated the excitonic coupling increased as the dye hydrophobicity increased. The KRM modeling supported the same trend for the hydrophobic dyes with higher values of the extracted hopping parameter $J_{1,2}$ for dyes with increased hydrophobicity. For hydrophilic dyes, the surface area served as a better predictor of aggregation and excitonic coupling strength for aggregates created by proximate covalent attachment to a template. Collectively, our results demonstrate that alternating hydrophobic structure of dyes covalently attached to DNA affords control of intermolecular distances and hence excitonic coupling strength in dye aggregates on a finer level than base pair separation. We

https://doi.org/10.1021/acs.jpcc.1c08981
J. Phys. Chem. C 2022, 126, 3475−3488

identified adjacent dimers of the strongly hydrophobic **SQ-Cl$_2$** dye that we ranked to be the best performing based on its extracted hopping parameter $J_{1,2}$ up to 132.2 meV (1065 cm^{-1}). Additional factors such as dye sterics and electrostatic factors play a role in tuning the dye alignment once dyes are brought together by the hydrophobic effect. Overall, we believe our findings will provide foundational guidance in rational design of dye aggregates that exhibit strong excitonic interactions and that are templated by DNA, including in larger aggregate networks assembled via more complex DNA scaffolds such as bricks and tiles.

■ ASSOCIATED CONTENT

Supporting Information

The Supporting Information is available free of charge at https://pubs.acs.org/doi/10.1021/acs.jpcc.1c08981.

Chemical synthesis of custom squaraine dyes; PAGE gel electrophoresis; absorption, fluorescence, and circular dichroism measurements; KRM modeling; and electrostatic surface potentials (PDF)

■ AUTHOR INFORMATION

Corresponding Authors

Ryan. D. Pensack − *Micron School of Materials Science & Engineering, Boise State University, Boise, Idaho 83725, United States;* orcid.org/0000-0002-1302-1770; Email: ryanpensack@boisestate.edu

Jeunghoon Lee − *Micron School of Materials Science & Engineering, Boise State University, Boise, Idaho 83725, United States; Department of Chemistry and Biochemistry, Boise State University, Boise, Idaho 83725, United States;* orcid.org/0000-0002-1909-4591; Email: jeunghoonlee@boisestate.edu

Authors

Olga A. Mass − *Micron School of Materials Science & Engineering, Boise State University, Boise, Idaho 83725, United States;* orcid.org/0000-0002-2309-2644

Christopher K. Wilson − *Micron School of Materials Science & Engineering, Boise State University, Boise, Idaho 83725, United States;* orcid.org/0000-0002-5197-6180

German Barcenas − *Micron School of Materials Science & Engineering, Boise State University, Boise, Idaho 83725, United States*

Ewald. A. Terpetschnig − *SETA BioMedicals, LLC, Urbana, Illinois 61801, United States*

Olena M. Obukhova − *State Scientific Institution "Institute for Single Crystals" of National Academy of Sciences of Ukraine, Kharkiv 61072, Ukraine*

Olga S. Kolosova − *State Scientific Institution "Institute for Single Crystals" of National Academy of Sciences of Ukraine, Kharkiv 61072, Ukraine*

Anatoliy L. Tatarets − *State Scientific Institution "Institute for Single Crystals" of National Academy of Sciences of Ukraine, Kharkiv 61072, Ukraine*

Lan Li − *Micron School of Materials Science & Engineering, Boise State University, Boise, Idaho 83725, United States; Center for Advanced Energy Studies, Idaho Falls, Idaho 83401, United States*

Bernard Yurke − *Micron School of Materials Science & Engineering, Boise State University, Boise, Idaho 83725, United States; Department of Electrical & Computer Engineering, Boise State University, Boise, Idaho 83725, United States;* orcid.org/0000-0003-3913-2855

William B. Knowlton − *Micron School of Materials Science & Engineering, Boise State University, Boise, Idaho 83725, United States; Department of Electrical & Computer Engineering, Boise State University, Boise, Idaho 83725, United States;* orcid.org/0000-0003-3018-2207

Complete contact information is available at: https://pubs.acs.org/10.1021/acs.jpcc.1c08981

Notes

The authors declare no competing financial interest.

■ ACKNOWLEDGMENTS

This research was supported wholly by the U.S. Department of Energy (DOE), Office of Basic Energy Sciences, Materials Sciences and Engineering Division and DOE's Established Program to Stimulate Competitive Research (EPSCoR) program under Award DE-SC0020089, except as follows: the circular dichroism spectrometer was made available through the Biomolecular Research Center (BRC) at Boise State, which is supported in part by the National Institutes of Health award no. P20GM109095, MJ Murdock Charitable Trust, and Idaho State Board of Education. We thank Dr. Natalya Hallstrom for the assistance with PAGE electrophoresis of squaraine-DNA constructs.

■ REFERENCES

(1) Brixner, T.; Hildner, R.; Köhler, J.; Lambert, C.; Würthner, F. Exciton Transport in Molecular Aggregates - from Natural Antennas to Synthetic Chromophore Systems. *Adv. Energy Mater.* **2017**, *7*, 1700236.

(2) Wasielewski, M. R. Self-Assembly Strategies for Integrating Light Harvesting and Charge Separation in Artificial Photosynthetic Systems. *Acc. Chem. Res.* **2009**, *42*, 1910−1921.

(3) Scholes, G. D.; Rumbles, G. Excitons in Nanoscale Systems. *Nat. Mater.* **2006**, *5*, 683−696.

(4) Ostroverkhova, O. Organic Optoelectronic Materials: Mechanisms and Applications. *Chem. Rev.* **2016**, *116*, 13279−13412.

(5) Yurke, B.; Kuang, W. Passive Linear Nanoscale Optical and Molecular Electronics Device Synthesis from Nanoparticles. *Phys. Rev. A: At., Mol., Opt. Phys.* **2010**, *81*, 033814.

(6) Graugnard, E.; Kellis, D. L.; Bui, H.; Barnes, S.; Kuang, W.; Lee, J.; Hughes, W. L.; Knowlton, W. B.; Yurke, B. DNA-Controlled Excitonic Switches. *Nano Lett.* **2012**, *12*, 2117−2122.

(7) Cannon, B. L.; Kellis, D. L.; Davis, P. H.; Lee, J.; Kuang, W.; Hughes, W. L.; Graugnard, E.; Yurke, B.; Knowlton, W. B. Excitonic and Logic Gates on DNA Brick Nanobreadboards. *ACS Photonics* **2015**, *2*, 398−404.

(8) Kellis, D. L.; Rehn, S. M.; Cannon, B. L.; Davis, P. H.; Graugnard, E.; Lee, J.; Yurke, B.; Knowlton, W. B. DNA-Mediated Excitonic Upconversion Fret Switching. *New J. Phys.* **2015**, *17*, 115007.

(9) Wang, S.; Lebeck, A. R.; Dwyer, C. Nanoscale Resonance Energy Transfer-Based Devices for Probabilistic Computing. *IEEE Micro* **2015**, *35*, 72−84.

(10) Sawaya, N. P. D.; Rappoport, D.; Tabor, D. P.; Aspuru-Guzik, A. Excitonics: A Set of Gates for Molecular Exciton Processing and Signaling. *ACS Nano* **2018**, *12*, 6410−6420.

(11) Kasha, M. Energy Transfer Mechanisms and the Molecular Exciton Model for Molecular Aggregates. *Radiat. Res.* **1963**, *20*, 55−70.

(12) McRae, E. G.; Kasha, M. The Molecular Exciton Model. In *Physical Processes in Radiation Biology*; Augenstein, L., Mason, R., Rosenberg, B., Eds.; Academic Press: New York, 1964; pp 23−42.

(13) Abramavicius, D.; Mukamel, S. Exciton Dynamics in Chromophore Aggregates with Correlated Environment Fluctuations. *J. Chem. Phys.* **2011**, *134*, 174504.
(14) Abramavicius, D.; Palmieri, B.; Mukamel, S. Extracting Single and Two-Exciton Couplings in Photosynthetic Complexes by Coherent Two-Dimensional Electronic Spectra. *Chem. Phys.* **2009**, *357*, 79−84.
(15) Abramavicius, D.; Palmieri, B.; Voronine, D. V.; Šanda, F.; Mukamel, S. Coherent Multidimensional Optical Spectroscopy of Excitons in Molecular Aggregates; Quasiparticle Versus Supermolecule Perspectives. *Chem. Rev.* **2009**, *109*, 2350−2408.
(16) Jelley, E. E. Molecular, Nematic and Crystal States of I: I-Diethyl−Cyanine Chloride. *Nature* **1937**, *139*, 631.
(17) Jelley, E. E. Spectral Absorption and Fluorescence of Dyes in the Molecular State. *Nature* **1936**, *138*, 1009−1010.
(18) Seeman, N. C. DNA in a Material World. *Nature* **2003**, *421*, 427−431.
(19) Rothemund, P. W. K. Folding DNA to Create Nanoscale Shapes and Patterns. *Nature* **2006**, *440*, 297−302.
(20) Ke, Y.; Ong, L. L.; Shih, W. M.; Yin, P. Three-Dimensional Structures Self-Assembled from DNA Bricks. *Science* **2012**, *338*, 1177−1183.
(21) Seeman, N. C. Structural DNA Nanotechnology: An Overview. *Methods Mol. Biol.* **2005**, *303*, 143−166.
(22) Wang, M.; Silva, G. L.; Armitage, B. A. DNA-Templated Formation of a Helical Cyanine Dye J-Aggregate. *J. Am. Chem. Soc.* **2000**, *122*, 9977−9986.
(23) Stadler, A. L.; Renikuntla, B. R.; Yaron, D.; Fang, A. S.; Armitage, B. A. Substituent Effects on the Assembly of Helical Cyanine Dye Aggregates in the Minor Groove of a DNA Template. *Langmuir* **2011**, *27*, 1472−1479.
(24) Seifert, J. L.; Connor, R. E.; Kushon, S. A.; Wang, M.; Armitage, B. A. Spontaneous Assembly of Helical Cyanine Dye Aggregates on DNA Nanotemplates. *J. Am. Chem. Soc.* **1999**, *121*, 2987−2995.
(25) Garoff, R. A.; Litzinger, E. A.; Connor, R. E.; Fishman, I.; Armitage, B. A. Helical Aggregation of Cyanine Dyes on DNA Templates: Effect of Dye Structure on Formation of Homo- and Heteroaggregates. *Langmuir* **2002**, *18*, 6330−6337.
(26) Boulais, É.; Sawaya, N. P. D.; Veneziano, R.; Andreoni, A.; Banal, J. L.; Kondo, T.; Mandal, S.; Lin, S.; Schlau-Cohen, G. S.; Woodbury, N. W.; et al. Programmed Coherent Coupling in a Synthetic DNA-Based Excitonic Circuit. *Nat. Mater.* **2018**, *17*, 159−166.
(27) Banal, J. L.; Kondo, T.; Veneziano, R.; Bathe, M.; Schlau-Cohen, G. S. Photophysics of J-Aggregate-Mediated Energy Transfer on DNA. *J. Phys. Chem. Lett.* **2017**, *8*, 5827−5833.
(28) Nicoli, F.; Roos, M. K.; Hemmig, E. A.; Di Antonio, M.; de Vivie-Riedle, R.; Liedl, T. Proximity-Induced H-Aggregation of Cyanine Dyes on DNA-Duplexes. *J. Phys. Chem. A* **2016**, *120*, 9941−9947.
(29) Markova, L. I.; Malinovskii, V. L.; Patsenker, L. D.; Häner, R. Synthesis and Properties of Squaraine-Modified DNA. *Org. Biomol. Chem.* **2012**, *10*, 8944−8947.
(30) Malinovskii, V. L.; Wenger, D.; Häner, R. Nucleic Acid-Guided Assembly of Aromatic Chromophores. *Chem. Soc. Rev.* **2010**, *39*, 410−422.
(31) Li, S.; Langenegger, S. M.; Häner, R. Control of Aggregation-Induced Emission by DNA Hybridization. *Chem. Commun.* **2013**, *49*, 5835−5837.
(32) Cunningham, P. D.; Kim, Y. C.; Díaz, S. A.; Buckhout-White, S.; Mathur, D.; Medintz, I. L.; Melinger, J. S. Optical Properties of Vibronically Coupled Cy3 Dimers on DNA Scaffolds. *J. Phys. Chem. B* **2018**, *122*, 5020−5029.
(33) Lee, W.; von Hippel, P. H.; Marcus, A. H. Internally Labeled Cy3/Cy5 DNA Constructs Show Greatly Enhanced Photo-Stability in Single-Molecule Fret Experiments. *Nucleic Acids Res.* **2014**, *42*, 5967−5977.
(34) Markova, L. I.; Malinovskii, V. L.; Patsenker, L. D.; Häner, R. J-Vs. H-Type Assembly: Pentamethine Cyanine (Cy5) as a near-Ir Chiroptical Reporter. *Chem. Commun.* **2013**, *49*, 5298−5300.
(35) Asanuma, H.; Fujii, T.; Kato, T.; Kashida, H. Coherent Interactions of Dyes Assembled on DNA. *J. Photochem. Photobiol., C* **2012**, *13*, 124−135.
(36) Heussman, D.; Kittell, J.; Kringle, L.; Tamimi, A.; von Hippel, P. H.; Marcus, A. H. Measuring local conformations and conformational disorder of (Cy3)2 dimer labeled DNA fork junctions using absorbance, circular dichroism and two-dimensional fluorescence spectroscopy. *Faraday Discuss.* **2019**, *216*, 211−235.
(37) Kringle, L.; Sawaya, N. P. D.; Widom, J.; Adams, C.; Raymer, M. G.; Aspuru-Guzik, A.; Marcus, A. H. Temperature-Dependent Conformations of Exciton-Coupled Cy3 Dimers in Double-Stranded DNA. *J. Chem. Phys.* **2018**, *148*, 085101.
(38) Asanuma, H.; Shirasuka, K.; Takarada, T.; Kashida, H.; Komiyama, M. DNA−Dye Conjugates for Controllable H* Aggregation1. *J. Am. Chem. Soc.* **2003**, *125*, 2217−2223.
(39) Häner, R.; Samain, F.; Malinovskii, V. L. DNA-Assisted Self-Assembly of Pyrene Foldamers. *Chem.—Eur. J.* **2009**, *15*, 5701−5708.
(40) Kashida, H.; Asanuma, H.; Komiyama, M. Alternating Hetero H Aggregation of Different Dyes by Interstrand Stacking from Two DNA-Dye Conjugates. *Angew. Chem., Int. Ed. Engl.* **2004**, *43*, 6522−6525.
(41) Ikeda, S.; Okamoto, A. Hybridization-Sensitive on-Off DNA Probe: Application of the Exciton Coupling Effect to Effective Fluorescence Quenching. *Chem.—Asian J.* **2008**, *3*, 958−968.
(42) Sohail, S. H.; Otto, J. P.; Cunningham, P. D.; Kim, Y. C.; Wood, R. E.; Allodi, M. A.; Higgins, J. S.; Melinger, J. S.; Engel, G. S. DNA Scaffold Supports Long-Lived Vibronic Coherence in an Indodicarbocyanine (Cy5) Dimer. *Chem. Sci.* **2020**, *11*, 8546−8557.
(43) Hart, S. M.; Chen, W. J.; Banal, J. L.; Bricker, W. P.; Dodin, A.; Markova, L.; Vyborna, Y.; Willard, A. P.; Häner, R.; Bathe, M.; et al. Engineering Couplings for Exciton Transport Using Synthetic DNA Scaffolds. *Chem* **2021**, *7*, 752−773.
(44) Cunningham, P. D.; Khachatrian, A.; Buckhout-White, S.; Deschamps, J. R.; Goldman, E. R.; Medintz, I. L.; Melinger, J. S. Resonance Energy Transfer in DNA Duplexes Labeled with Localized Dyes. *J. Phys. Chem. B* **2014**, *118*, 14555−14565.
(45) Garo, F.; Häner, R. A DNA-Based Light-Harvesting Antenna. *Angew. Chem., Int. Ed. Engl.* **2012**, *51*, 916−919.
(46) Fujii, T.; Kashida, H.; Asanuma, H. Analysis of Coherent Heteroclustering of Different Dyes by Use of Threoninol Nucleotides for Comparison with the Molecular Exciton Theory. *Chem.—Eur. J.* **2009**, *15*, 10092−10102.
(47) Kashida, H.; Tanaka, M.; Baba, S.; Sakamoto, T.; Kawai, G.; Asanuma, H.; Komiyama, M. Covalent Incorporation of Methyl Red Dyes into Double-Stranded DNA for Their Ordered Clustering. *Chem.—Eur. J.* **2006**, *12*, 777−784.
(48) Probst, M.; Wenger, D.; Biner, S. M.; Häner, R. The DNA Three-Way Junction as a Mould for Tripartite Chromophore Assembly. *Org. Biomol. Chem.* **2012**, *10*, 755−759.
(49) Mazuski, R. J.; Díaz, S. A.; Wood, R. E.; Lloyd, L. T.; Klein, W. P.; Mathur, D.; Melinger, J. S.; Engel, G. S.; Medintz, I. L. Ultrafast Excitation Transfer in Cy5 DNA Photonic Wires Displays Dye Conjugation and Excitation Energy Dependency. *J. Phys. Chem. Lett.* **2020**, *11*, 4163−4172.
(50) Barclay, M. S.; Roy, S. K.; Huff, J. S.; Mass, O. A.; Turner, D. B.; Wilson, C. K.; Kellis, D. L.; Terpetschnig, E. A.; Lee, J.; Davis, P. H.; et al. Rotaxane Rings Promote Oblique Packing and Extended Lifetimes in DNA-Templated Molecular Dye Aggregates. *Chem. Commun.* **2021**, *4*, 19.
(51) Cannon, B. L.; Kellis, D. L.; Patten, L. K.; Davis, P. H.; Lee, J.; Graugnard, E.; Yurke, B.; Knowlton, W. B. Coherent Exciton Delocalization in a Two-State DNA-Templated Dye Aggregate System. *J. Phys. Chem. A* **2017**, *121*, 6905−6916.
(52) Cannon, B. L.; Patten, L. K.; Kellis, D. L.; Davis, P. H.; Lee, J.; Graugnard, E.; Yurke, B.; Knowlton, W. B. Large Davydov Splitting and Strong Fluorescence Suppression: An Investigation of Exciton

https://doi.org/10.1021/acs.jpcc.1c08981
J. Phys. Chem. C 2022, 126, 3475−3488

Delocalization in DNA-Templated Holliday Junction Dye Aggregates. *J. Phys. Chem. A* **2018**, *122*, 2086−2095.
(53) Huff, J. S.; Davis, P. H.; Christy, A.; Kellis, D. L.; Kandadai, N.; Toa, Z. S. D.; Scholes, G. D.; Yurke, B.; Knowlton, W. B.; Pensack, R. D. DNA-Templated Aggregates of Strongly Coupled Cyanine Dyes: Nonradiative Decay Governs Exciton Lifetimes. *J. Phys. Chem. Lett.* **2019**, *10*, 2386−2392.
(54) Mass, O. A.; Wilson, C. K.; Roy, S. K.; Barclay, M. S.; Patten, L. K.; Terpetschnig, E. A.; Lee, J.; Pensack, R. D.; Yurke, B.; Knowlton, W. B. Exciton Delocalization in Indolenine Squaraine Aggregates Templated by DNA Holliday Junction Scaffolds. *J. Phys. Chem. B* **2020**, *124*, 9636−9647.
(55) Brown, S. B.; Shillcock, M.; Jones, P. Equilibrium and Kinetic Studies of the Aggregation of Porphyrins in Aqueous Solution. *Biochem. J.* **1976**, *153*, 279−285.
(56) Hamada, K.; Mitshuishi, M.; Ohira, M.; Miyazaki, K. Positional Effects of a Trifluoromethyl Group on the Aggregation of Azo Dyes in Aqueous Solutions. *J. Phys. Chem.* **1993**, *97*, 4926−4929.
(57) Mukerjee, P.; Ghosh, A. K. Thermodynamic Aspects of the Self-Association and Hydrophobic Bonding of Methylene Blue. Model System for Stacking Interactions. *J. Am. Chem. Soc.* **1970**, *92*, 6419−6424.
(58) Murakami, K. Thermodynamic and Kinetic Aspects of Self-Association of Dyes in Aqueous Solution. *Dyes Pigm.* **2002**, *53*, 31−43.
(59) Patil, K.; Pawar, R.; Talap, P. Self-Aggregation of Methylene Blue in Aqueous Medium and Aqueous Solutions of Bu4nbr and Urea. *Phys. Chem. Chem. Phys.* **2000**, *2*, 4313−4317.
(60) Takahashi, D.; Oda, H.; Izumi, T.; Hirohashi, R. Substituent Effects on Aggregation Phenomena in Aqueous Solution of Thiacarbocyanine Dyes. *Dyes Pigm.* **2005**, *66*, 1−6.
(61) McKerrow, A. J.; Buncel, E.; Kazmaier, P. M. Aggregation of squaraine dyes: Structure-property relationships and solvent effects. *Can. J. Chem.* **1995**, *73*, 1605−1615.
(62) Markova, L. I.; Terpetschnig, E. A.; Patsenker, L. D. Comparison of a Series of Hydrophilic Squaraine and Cyanine Dyes for Use as Biological Labels. *Dyes Pigm.* **2013**, *99*, 561−570.
(63) Biaggne, A.; Knowlton, W. B.; Yurke, B.; Lee, J.; Li, L. Substituent Effects on the Solubility and Electronic Properties of the Cyanine Dye Cy5: Density Functional and Time-Dependent Density Functional Theory Calculations. *Molecules* **2021**, *26*, 524.
(64) Barcenas, G.; Biaggne, A.; Mass, O. A.; Wilson, C. K.; Obukhova, O. M.; Kolosova, O. S.; Tatarets, A. L.; Terpetschnig, E.; Pensack, R. D.; Lee, J.; et al. First-Principles Studies of Substituent Effects on Squaraine Dyes. *RSC Adv.* **2021**, *11*, 19029−19040.
(65) Fothergill, J. W.; Hernandez, A. C.; Knowlton, W. B.; Yurke, B.; Li, L. Ab Initio Studies of Exciton Interactions of Cy5 Dyes. *J. Phys. Chem. A* **2018**, *122*, 8989−8997.
(66) Hanwell, M. D.; Curtis, D. E.; Lonie, D. C.; Vandermeersch, T.; Zurek, E.; Hutchison, G. R. Avogadro: An Advanced Semantic Chemical Editor, Visualization, and Analysis Platform. *J. Cheminf.* **2012**, *4*, 17.
(67) Rappe, A. K.; Casewit, C. J.; Colwell, K. S.; Goddard, W. A.; Skiff, W. M. Uff, a Full Periodic Table Force Field for Molecular Mechanics and Molecular Dynamics Simulations. *J. Am. Chem. Soc.* **1992**, *114*, 10024−10035.
(68) Zhao, Y.; Truhlar, D. G. The M06 Suite of Density Functionals for Main Group Thermochemistry, Thermochemical Kinetics, Noncovalent Interactions, Excited States, and Transition Elements: Two New Functionals and Systematic Testing of Four M06-Class Functionals and 12 Other Functionals. *Theor. Chem. Acc.* **2008**, *120*, 215−241.
(69) Frisch, M. J.; Trucks, G. W.; Schlegel, H. B.; Scuseria, G. E.; Robb, M. A.; Cheeseman, J. R.; Scalmani, G.; Barone, V.; Petersson, G. A.; Nakatsuji, H., et al. *Gaussian 16* Revision C.01; Gaussian Inc.: Wallingford, CT, 2016.
(70) Marenich, A. V.; Cramer, C. J.; Truhlar, D. G. Universal Solvation Model Based on Solute Electron Density and on a Continuum Model of the Solvent Defined by the Bulk Dielectric Constant and Atomic Surface Tensions. *J. Phys. Chem. B* **2009**, *113*, 6378−6396.
(71) Spano, F. C. The Spectral Signatures of Frenkel Polarons in H- and J-Aggregates. *Acc. Chem. Res.* **2010**, *43*, 429−439.
(72) Huff, J. S.; Turner, D. B.; Mass, O. A.; Patten, L. K.; Wilson, C. K.; Roy, S. K.; Barclay, M. S.; Yurke, B.; Knowlton, W. B.; Davis, P. H.; et al. Excited-State Lifetimes of DNA-Templated Cyanine Dimer, Trimer, and Tetramer Aggregates: The Role of Exciton Delocalization, Dye Separation, and DNA Heterogeneity. *J. Phys. Chem. B* **2021**, *125*, 10240−10259.
(73) Kühn, O.; Renger, T.; May, V. Theory of Exciton-Vibrational Dynamics in Molecular Dimers. *Chem. Phys.* **1996**, *204*, 99−114.
(74) Czikklely, V.; Forsterling, H. D.; Kuhn, H. Extended Dipole Model for Aggregates of Dye Molecules. *Chem. Phys. Lett.* **1970**, *6*, 207−210.
(75) Michail, E.; Schreck, M. H.; Holzapfel, M.; Lambert, C. Exciton Coupling Effects on the Two-Photon Absorption of Squaraine Homodimers with Varying Bridge Units. *Phys. Chem. Chem. Phys.* **2020**, *22*, 18340−18350.
(76) Tsuzuki, S.; Honda, K.; Uchimaru, T.; Mikami, M.; Tanabe, K. Origin of Attraction and Directionality of the π/π Interaction: Model Chemistry Calculations of Benzene Dimer Interaction. *Am. Chem. Soc.* **2002**, *124*, 104−112.
(77) Anslyn, E. V.; Dougherty, D. A. *Modern Physical Organic Chemistry*; University Science Books: Sausalito, California, 2005.
(78) Dyson, H. J.; Wright, P. E.; Scheraga, H. A. The Role of Hydrophobic Interactions in Initiation and Propagation of Protein Folding. *Proc. Natl. Acad. Sci. U.S.A.* **2006**, *103*, 13057.
(79) Hunter, C. A.; Sanders, J. K. M. The Nature Of .Pi.-.Pi. Interactions. *J. Am. Chem. Soc.* **1990**, *112*, 5525−5534.

https://doi.org/10.1021/acs.jpcc.1c08981
J. Phys. Chem. C 2022, 126, 3475−3488